Powder Technology 312 (2017) 1–10

Contents lists available at ScienceDirect

Powder Technology

journal homepage: www.elsevier.com/locate/powtec

A new rapid and economical one-step method for preparing SiO_2 aerogels using supercritical extraction

Xiaodong Wu [a,b,d], Gaofeng Shao [a,b,d], Sijia Liu [a,b,d], Xiaodong Shen [a,b,d,*], Sheng Cui [a,b,d,*], Xiangbao Chen [c]

[a] College of Materials Science and Engineering, Nanjing Tech University, Nanjing 210009, China
[b] Jiangsu Collaborative Innovation Center for Advanced Inorganic Function Composites, Nanjing Tech University, Nanjing 210009, China
[c] Beijing Institute of Aeronautic Materials, Beijing 100095, China
[d] Advanced Materials Institute of Nanjing Tech University in Suqian, Suqian 223800, China

ARTICLE INFO

Article history:
Received 19 November 2016
Received in revised form 21 January 2017
Accepted 25 January 2017
Available online 27 January 2017

Keywords:
Rapid supercritical extraction
Silica aerogel
Heat treatment
Pore structures
Thermal conductivity

ABSTRACT

Monolithic silica aerogels (SiO_2) are prepared using the tetraethylorthosilicate (TEOS) as precursor via a rapid supercritical extraction method (RSCE). The effect of heat treatment on the textural and physical characteristics of RSCE-samples are compared with those of the other two conventional supercritical extraction method, i.e. the alcohol supercritical extraction (ASCE) and CO_2 supercritical extraction (CSCE). This new RSCE method offers many distinct advantages. The precursor recipe employs TEOS, ethanol, water, diluted hydrochloric acid to catalyst hydrolysis, and ammonia to accelerate the condensation rate. One advantage is the relative simplicity of this method: liquid precursors are poured into the supercritical ethanol drying apparatus following the hydrolysis of the TEOS and the solutions are directly sent to the supercritical extraction point of ethanol without previous aging and solvent exchanges procedures as would be the case for conventional aerogel. Thus, it is much more cost-saving and it produces little waste during the overall fabrication. The total fabrication time from mixing the precursors to taking out can be shortened to as low as 6 h, which is much less time consuming than the conventional ones (usually ca. 4–7 days). All the as-dried SiO_2 samples derived from different methods are essentially amorphous, and SiO_2 crystallization first occurs for the ASCE sample at 1100 °C. The average pore diameters of the as-dried ASCE, CSCE and RSCE samples are 12.70 nm, 14.97 nm and 13.80 nm, respectively, which is consistent with the results of transmission electron microscopy (TEM) analysis. The specific surface area of the as-dried RSCE silica aerogel may reach 915.9 m^2/g after 700 °C, which is larger than the other two samples. The thermal conductivities of the different fiber reinforced RSCE SiO_2 aerogel composites are ca. 0.027 $W\ m^{-1}\ K^{-1}$, comparable to the ASCE and CSCE aerogel composites. The RSCE method can also be well applied to the fabrication of aerogels based on other precursor recipes.

1. Introduction

Silica aerogels are nanoporous materials with distinct nanoparticles and nanopores, which have high porosity (>99%), low thermal conductivity (<0.02 $W\ m^{-1}\ K^{-1}$), high specific surface area (>1000 m^2/g) and low densities (<3 mg/cm^3) [1–4]. Thus, they have been attractive for use in a large number of applications, such as drug delivery systems, chemical sensors, thermal insulations, catalyst barriers and comet dust collectors and other areas [5–8]. Silica aerogels are usually made using the sol-gel technique, and are dried in such a way to avoid pore collapse, leaving an intact solid nanostructure in a material that is 90–99% air by volume [9,10]. Thus, the key to making an aerogel is to choose a good drying method without making any damages to the original skeleton. As is well known, there are three drying methods used to fabricate an aerogel, which are ambient pressure drying, freeze-drying and supercritical extraction [11].

Ambient pressure drying is designed to dry the gel under ambient pressure, which always requires chemical processing with a lengthy solvent exchange either to reduce the capillary forces acting on the nanostructure or to strengthen the nanostructure to withstand the capillary forces [12–15]. The main advantage of the ambient drying method is that one does not need expensive and potentially dangerous high-temperature and high-pressure equipment; however, this method is time-consuming, and the procedures can be complicated due to the consecutive chemical modification procedures. The freeze-drying method was first invented by Pajonk et al. [16], and this technique removes excess solvent through sublimation. It avoids the generation of a solid-liquid interface, which results in capillary forces. Thus, many researchers have since attempted to use this method to fabricate aerogels. The freeze-drying method, always results in powders rather than

* Corresponding authors at: College of Materials Science and Engineering, Nanjing Tech University, Nanjing 210009, China.
E-mail addresses: xdshen@njtech.edu.cn (X. Shen), cui2002sheng@126.com (S. Cui).

http://dx.doi.org/10.1016/j.powtec.2017.01.067
0032-5910/

aerogels; thus, the as-prepared samples are also called cryogels. The most frequently used method to make aerogels is the supercritical method, which involves alcohol supercritical extraction (ASCE) and CO_2 supercritical extraction (CSCE). The ASCE method uses a high temperature (above 260 °C) and high pressure (above 8 MPa) that is beyond the critical point of the alcohol solvent in an autoclave or other pressurized vessel [17–19]. Many studies have shown that the processing parameters including solvent fill volume, pre-pressure, temperature and pressure, greatly affect the textural and physical properties of the as-dried aerogels [20]. The CSCE method is based on the supercritical extraction of CO_2, which has a much lower critical-point temperature than the alcohol mixture [21–23]. Thus, it is considered as a much safer way to create an aerogel. These supercritical methods both require a series of aging and solvent exchanges for the wet gels. This is especially true for the CSCE method because it is a low-temperature supercritical extraction system. These two procedures occupy the majority of the fabrication time required to produce an aerogel. On the other hand, during the aging and solvent exchange process, copious volumes of solvent, such as ethanol and n-hexane, are used and a large amount of environmentally harmful waste is produced. Thus, an attempt to find a way of fabricating aerogels via a one-step precursor to the aerogel processes is worthwhile. Anderson et al. [24–26] attempted to develop a one-pot method to prepare different types of oxide aerogels using a hydraulic hot press acting on a steel mold. The fabrication time can be much decreased and the samples can be made hydrophobic and transparent through this one-step method. However, the dimensions of the derived samples are limited and the specific surface areas are smaller than the samples obtained from the conventional ASCE and CSCE methods, which is unfavorable for many applications, including high-temperature thermal insulations and catalyst barriers. Herein, we present a new procedure for producing silica aerogels using the rapid supercritical extraction method (RSCE) and completed within as little as 6 h; this method doesn't need a solvent exchange process, produces little waste, and retains the superior textural and physical properties characteristic of the conventional ASCE and CSCE drying methods. The as-prepared samples have a large specific surface area at elevated temperatures, and the effects of heat treatment on the properties of the silica aerogels are evaluated in detail and compared with ASCE and CSCE samples in this article.

2. Experimental procedures

2.1. Synthesis

Tetraethylorthosilicate (TEOS, analytical pure, Sinopharm Chemical Reagent Co., Ltd.) was used as silicon source. Hydrochloric acid (HCl, 1 mol L^{-1}, Shanghai Zhongshi Chemical Co., Ltd) and ammonia solution ($NH_3 \cdot H_2O$, 0.3 mol L^{-1}, Wuxi City Yasheng Chemical Co., Ltd.) were used as catalysts. Deionized water (homemade) was used as hydrolysis agent and absolute ethyl alcohol (EtOH, analytical pure, Wuxi City Yasheng Chemical Co., Ltd.) as solvent. All of the reactants and solvents were used as received without further purification. In a typical synthesis, TEOS (22.4 mL, 0.1 mol) was first dissolved in a mixture of water (7.2 mL, 0.4 mol) and ethanol (92 mL, 1.6 mol). Secondly, appropriate amount of HCl (0.3 mL, 0. 3 mmol) was added to the mixture, stirring for about 60 min at 50 °C for full hydrolysis. Thirdly, desired amount of $NH_3 \cdot H_2O$ (3 mL, 0.9 mmol) was added to the solution. The solution was further stirred for 5 min, after which the solutions were directly placed in an autoclave using a container with volume of 0.5 L. The RSCE drying apparatus and the processing parameters are shown in Fig. 1. After the vessel was sealed, it was firstly purged by N_2 three times to drive out the air, and then it was pressurized to 4 ± 0.2 MPa by N_2. The temperature of the vessel was first raised from room temperature to 270 °C with a heating rate of 2 °C/min, and maintained at that level for 2 h. The automatic vessel pressure was controlled at 10 ± 0.2 MPa. At the end, the vent valve was opened to depressurize the vessel to ambient pressure with a depressurization rate of ca. 20 bar/h by regulating the back pressure regulator, thus affording the RSCE-SiO_2 aerogel. The total processing time was as short as 6 h, as indicated by Fig. 1(b). In order to evaluate the heat treatment on the textural and physical properties on silica aerogels with different drying methods including RSCE, ASCE and CSCE samples, the ASCE and CSCE silica aerogels are fabricated with the conventional sol-gel technique, including aging, solvent exchange and supercritical drying using the same recipe. The wet gels were both aged at room temperature for 1 d and subsequently soaked in a bath of absolute ethanol in an oven of 50 °C for 5 d to exchange the water and reaction byproducts from the pores of the materials. The total time from mixing the precursors to obtaining the aerogels was ca. 7 d for these two conventional supercritical drying methods. It is noted that the as-dried silica aerogels are denoted as ASCE-25, CSCE-25 and RSCE-25, respectively, and the RSCE sample heat treated at 700 °C (heating rate of 3 °C/min) with holding time of 2 h is denoted as RSCE-700, as is the same case for other samples.

2.2. Characterizations

Thermal gravimetric analysis (TGA) and differential scanning calorimetry analysis (DSC) were performed by NETZSCH STA449C. Thermogravimetric analyzer under a constant nitrogen flow of 30 mL/min at a heating rate of 10 °C/min to 1200 °C. X-ray diffraction (XRD) patterns were recorded using a Rigaku Smart Lab 3000, a diffractometer with CuKα_1 radiation ($\lambda = 0.15406$ nm). The X-ray tube was operated at 35 kV and 30 mA. Scanning electron microscopy (SEM) was conducted using a LEO-1530VP field emission scanning electron microscope. Photographs of the aerogels were taken with a transmission electron microscope (TEM) using JEOL JEM-2100 (UHR) operating at the acceleration voltage of 200 kV. Surface areas, pore volume and pore distribution

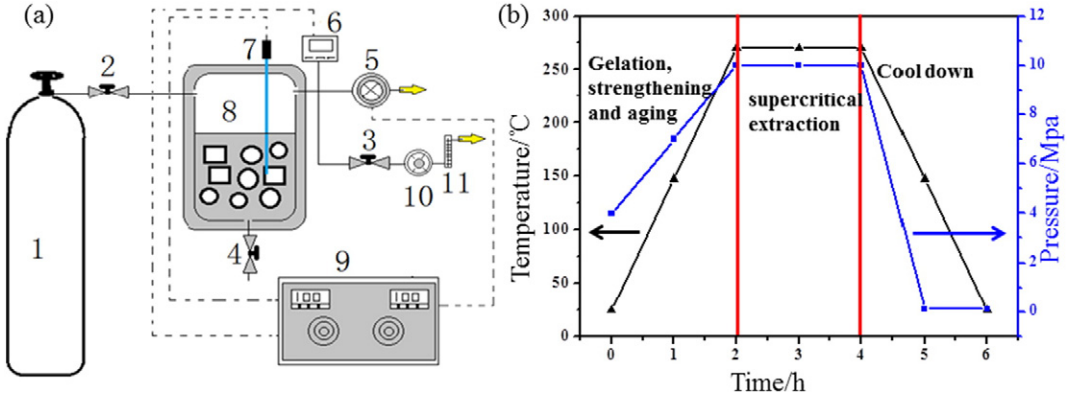

Fig. 1. (a) Diagram of the supercritical ethanol drying apparatus: (1) N_2 cylinder; (2) N_2 inlet valve; (3) vent valve; (4) liquid vent valve; (5) automatic pressure control valve; (6) pressure sensor; (7) thermal couple; (8) vessel; (9) controller; (10) back pressure regulator; (11) flow meter, and Fig. 1 (b) processing parameters used during RSCE process.

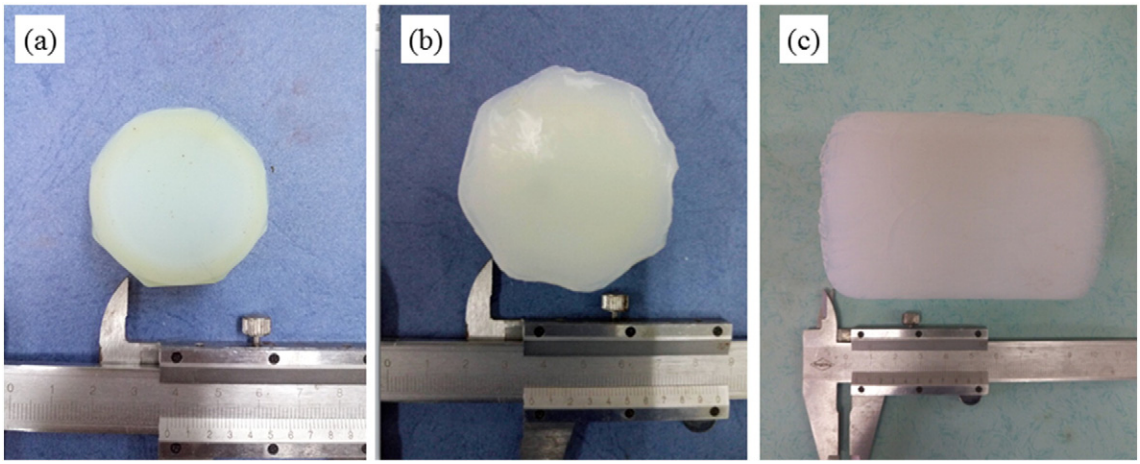

Fig. 2. Photographs of SiO_2 aerogels derived from different supercritical drying methods (a) ASCE-25, (b) CSCE-25 and (c) RSCE-25.

were measured by nitrogen adsorption/desorption measurement by using a 3Flex Version 3.01 surface area and pore distribution analyzer after the samples were degassed in a vacuum at 300 °C for 5 h. FTIR spectra was taken with a Nicolet Avatar 330 FT-IR with a Smart Orbit Diamond ATR attachment using a resolution of 4 cm^{-1} and 32 scans. The thermal conductivities of the fiber reinforced aerogels were investigated by the measuring apparatus (TPS2500, Hot Disk, Sweden) using a transient plane heat source method at room temperature of 25 °C.

3. Results and discussion

Fig. 1 shows a diagram of the RSCE drying apparatus and the processing parameters used during the RSCE process. As shown in Fig. 1(a), the RSCE drying apparatus is simple and convenient and is actually a sealed reactor capable of high temperature and high pressure. The processing parameters in Fig. 1(b) show the total process for fabricating an RSCE aerogel, which can be divided into three two-hour stages. The first 2 h are for gelation, strengthening and aging. After the liquid solution is poured into the vessel, it gels quickly with an increase in temperature and pressure; thus, it undergoes an aging and strengthening stage during the high-temperature and high-pressure conditions within the vessel, whereas this process occurs at an ambient pressure (1 bar) and low temperature (<50 °C) for the ASCE and CSCE methods. The second 2 h are for supercritical extraction, during which stage the ethanol becomes a supercritical fluid, with no solid-liquid interface and no capillary forces acting on the skeleton. The third stage which involves the cool down stage that is necessary for subsequent manipulation. Thus, the total processing time can be shortened to 6 h, which is substantially faster than the conventional ASCE and CSCE methods.

Fig. 2 exhibits photographs of the ASCE, CSCE and RSCE silica aerogels. The ASCE and CSCE samples are somewhat white, opaque and smooth, while the RSCE sample has a relatively optically transparent appearance.

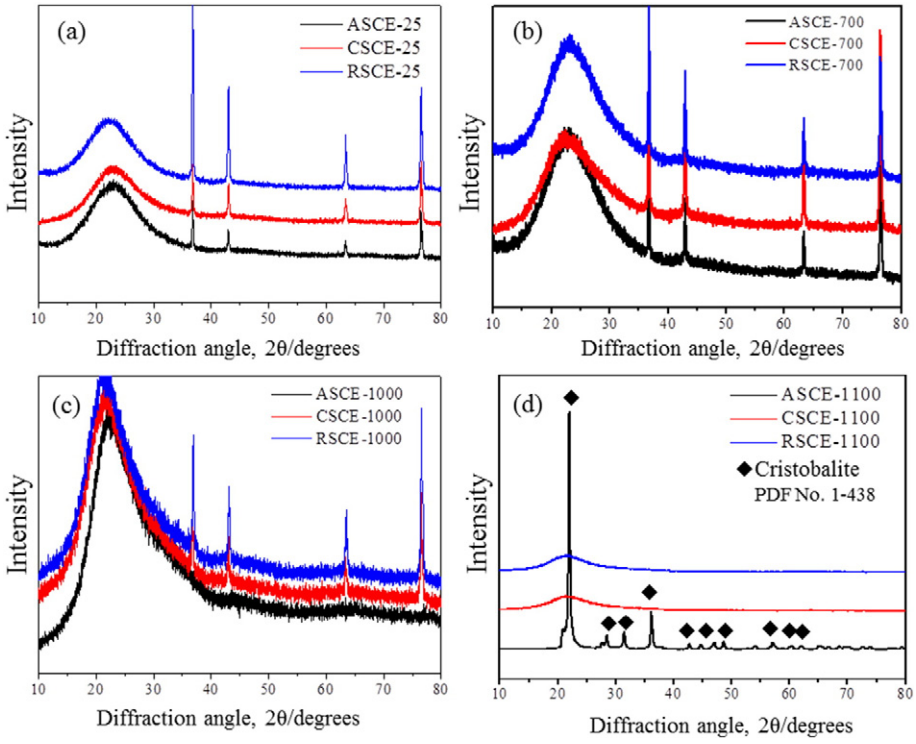

Fig. 3. XRD patterns of SiO_2 aerogels heat treated at different temperatures using different supercritical drying methods (a) as-dried, (b) 700 °C, (c) 1000 °C, and (d) 1100 °C. Note that the sharp peaks at 37°, 43°, 63° and 76° are due to the aluminum sample holder.

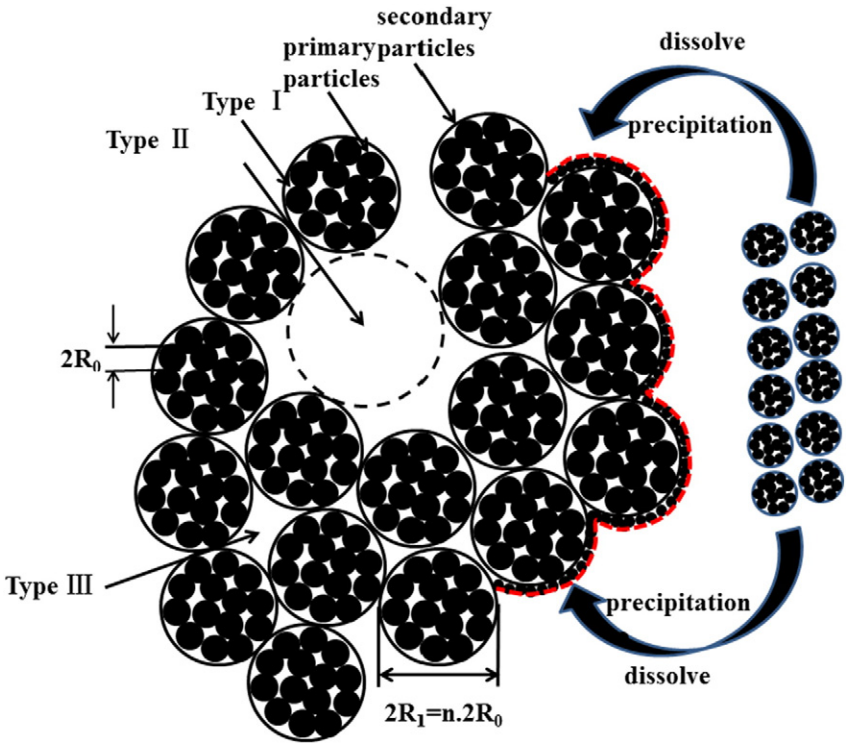

Fig. 4. Schematic diagram of SiO_2 sols growth in the supercritical drying process.

The RSCE sample is approximately 10 cm in length with a diameter that is larger than 5 cm, and it can be easily fabricated on a large scale when necessary. In our experiments, we have adjusted the TEOS concentration (10%, 15%, 20%, 25%, 30%, 40% and 50%) in the total solution. Results show that the 10% recipe forms powders rather than an aerogel. The 50% recipe possesses a much higher bulk density than the conventional aerogels, which is also not appropriate for aerogel based thermal insulation usage. The 15% recipe forms an aerogel with many cracks on its surface while the other four samples keep monoliths. In addition, the bulk densities of these five samples are 0.116 g/cm^3, 0.084 g/cm^3, 0.122 g/cm^3, 0.145 g/cm^3, and 0.219 g/cm^3, respectively. Photographs of the five samples (The original shapes of these five samples are cylindrical just as shown in Fig. 2(c)) are shown in Fig. S1. It is found that with the increase of TEOS concentration, the samples become more transparent due to a

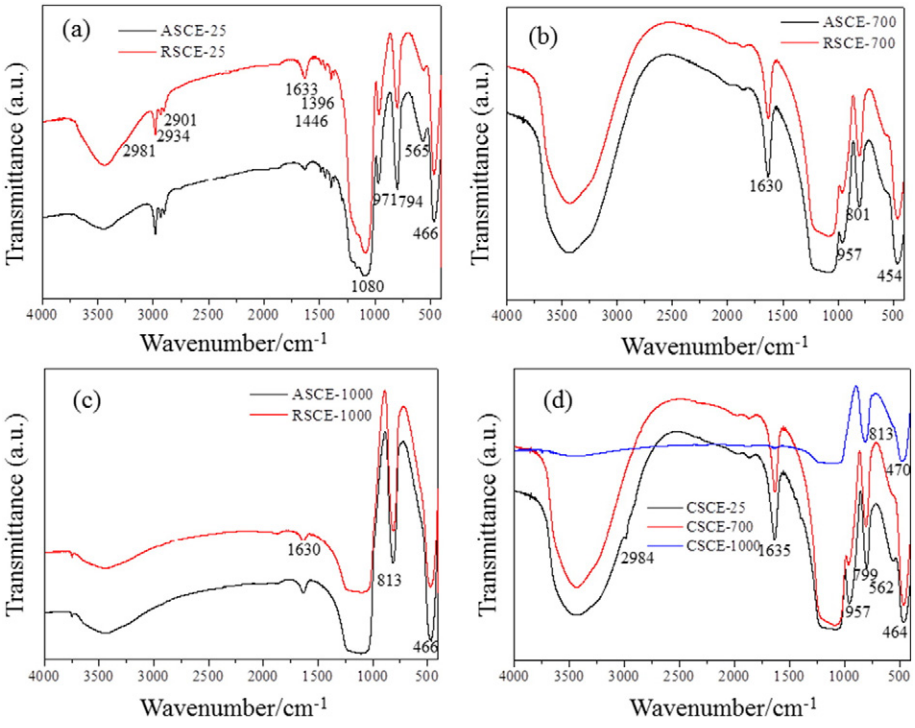

Fig. 5. FTIR spectra of SiO_2 aerogels derived from different supercritical drying methods and heat treatment temperatures.

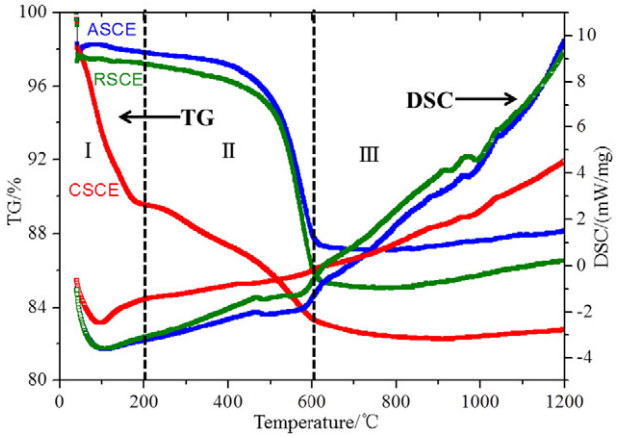

Fig. 6. TG and DSC curves of as-dried silica aerogels under flowing nitrogen derived from different drying methods.

much more concentrated pore size distribution (Fig. S2 left top inlet) within the aerogel structures. Fig. S2 shows the nitrogen sorption isotherms and the pore size distribution of the as-dried silica aerogels with different TEOS concentrations. Note that the 40% recipe possesses a significantly larger volume adsorbed (vertical coordinate) than other samples; however, it doesn't mean that the sample possesses the largest specific surface area since the specific surface area is correlated with the saturated adsorption capacity rather than volume adsorbed. The specific surface area and bulk density vary with the TEOS concentration, as is shown in Fig. S3. The largest BET area corresponds to the 20% recipe, which also possesses the largest porosity; thus, the TEOS concentration used for this study is 20% within the full article. The theoretical density of a silica aerogel can be calculated using the following equation:

$$\rho = \frac{M_{SiO_2}}{V_{total}} = \frac{M_{SiO_2}}{V_{EtOH} + V_{TEOS} + V_{H_2O}} \quad (1)$$

The bulk densities of the three ASCE, CSCE and RSCE silica aerogels are 0.14 g/cm^3, 0.20 g/cm^3 and 0.09 g/cm^3, which are larger than the theoretical density (0.05 g/cm^3); these densities are caused by the volume shrinkage during the solvent exchange period and the decreased total volume when mixing the solutions. Because the skeletal density of the aerogels is ca. 2.05 g/cm^3, the porosities calculated are 93.2%, 91.2% and 95.6%. Thus, the RSCE sample has the largest porosity of the three samples, and it can be fabricated on a large scale and in different shapes, as indicated by Fig. 2(c). The largest porosity can be explained by the aerogel fabrication process; the precursor solution undergoes hydrolysis and condensation when using the two-step process. As is well known, the two processes can be described by the following reactions:

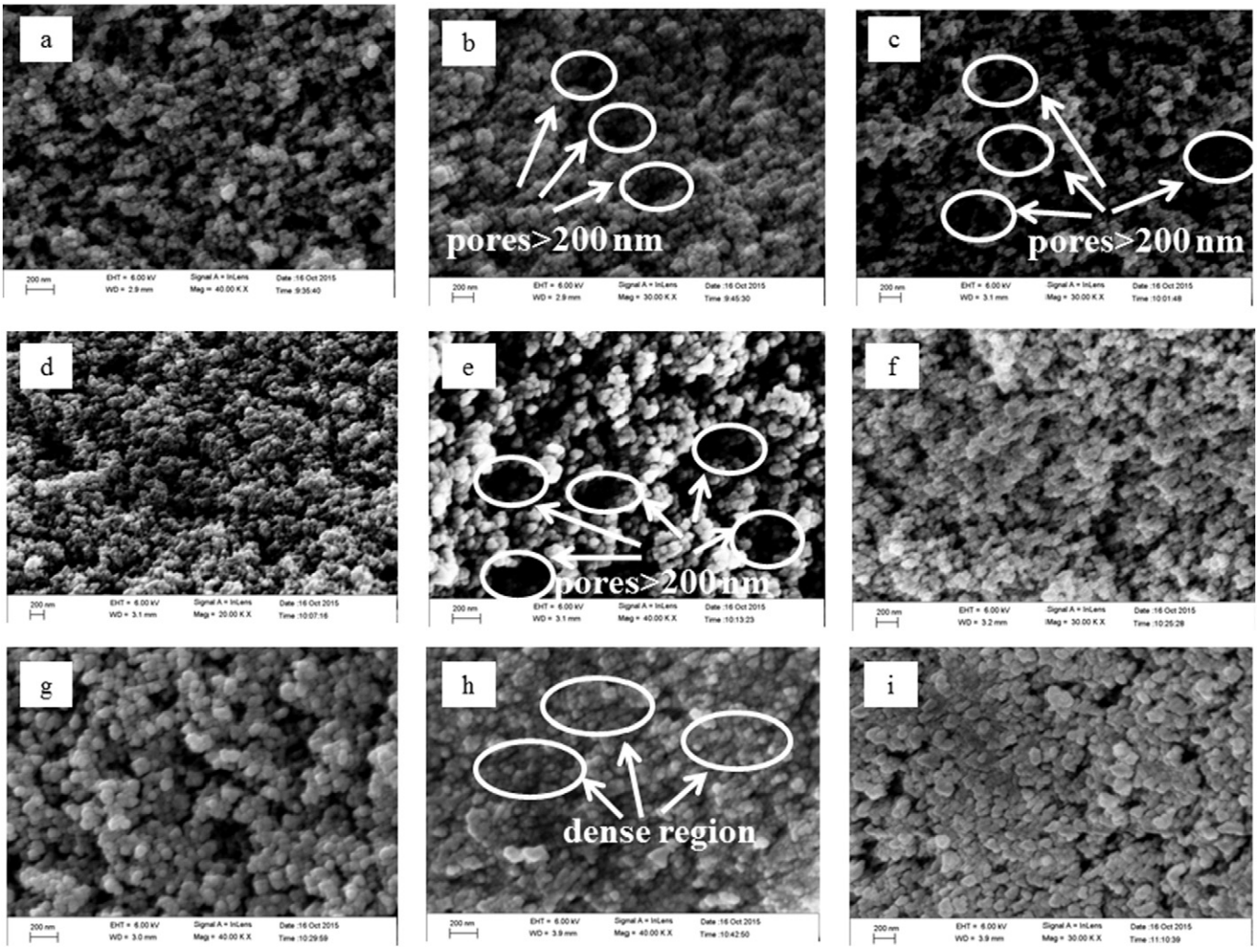

Fig. 7. SEM images of silica aerogels derived from different drying methods and heat treatment temperatures: (a) ASCE-25; (b) CSCE-25; (c) RSCE-25; (d) ASCE-700; (e) CSCE-700; (f) RSCE-700; (g) ASCE-1000; (h) CSCE-1000 and (i) RSCE-1000.

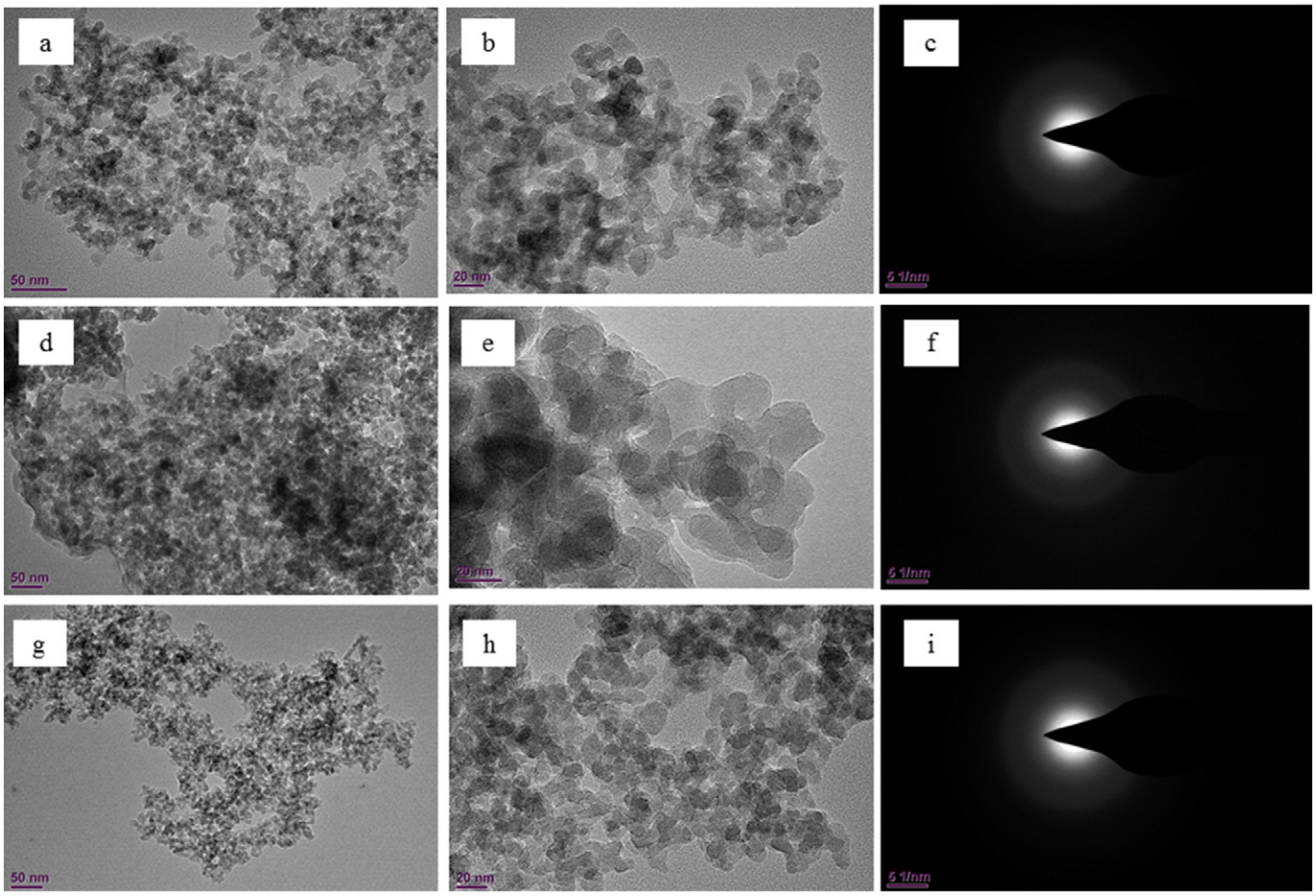

Fig. 8. TEM images and diffraction rings of silica aerogels heat treated at 1000 °C derived from different drying methods: (a–c) ASCE-1000; (d–f) CSCE-1000 and (g–i) RSCE-1000.

Hydrolysis:

$$Si(OC_2H_5)_4 + nH_2O \rightarrow Si(OC_2H_5)_{4-n}(OH)_n + nC_2H_5OH \quad (1)$$

Condensation:

$$\text{-Si-OH} + (HO)_n + Si(OC_2H_5)_{4-n} \rightarrow \text{-Si-O-}Si(OH)_{n-1}(OC_2H_5)_{4-n} + H_2O \quad (2)$$

The bulk density can be varied by adjusting the silica mass ratio in the precursor solution, which is appealing for further applications, including scale-up of the process.

Fig. 3 presents the XRD patterns of the SiO_2 aerogels heat treated at different temperatures using different supercritical drying methods. The sharp, intense peaks at 37°, 43°, 63° and 76° shown in Fig. 3 are due to the aluminum sample plate. For the as-dried samples, there is a single broad diffraction peak at ca. 22°, which corresponds to amorphous silica, and no other phases are observed within the three samples. With increasing heat-treatment temperatures, the broad peak becomes sharper, whereas there are no new phases below 1000 °C. When the heat-treatment temperature increases to 1100 °C, the cristobalite phase begins to emerge in the ASCE sample, as indicated in Fig. 3(d). The CSCE sample remains amorphous silica at temperatures as high as 1100 °C, which is due to the lower supercritical temperature (ca. 50 °C) of this method compared to the ASCE and RSCE methods; thus, the driving force of crystallization is decreased for of the as-prepared sample. However, the RSCE sample also remains amorphous at such a high temperature, which reveals that the RSCE process inhibits silica crystallization, and this is favorable for larger specific surface areas at elevated temperatures. This phenomenon can be explained by the different reaction mechanisms of the ASCE and RSCE methods. In the ASCE method, the wet gel is formed at room temperature and ambient pressure. The gel skeleton is somewhat strengthened via the aging and solvent exchange processes; whereas some —Si—OH remains that does not undergo condensation reactions within the gel skeleton because of its rigid network and steric effects. According to the Ostwald-Freundlich's [27] equation, the solubility of a solid material is relative to the size of its particles and the temperature, as described by the following equation:

$$s = s_0 \exp\left(2\gamma_{s1}V_m/R_gTr\right) \quad (3)$$

where S_0 is the solubility at a flat interface ($r = \infty$), γ_{sl} is the surface tension, V_m is the molar volume, R_g is the ideal gas constant, T is the temperature and r is the radius of curvature along the principal sections of the curved interface. Thus, the solubility increases with a decrease in particle

Table 1
Pore structures of different SiO_2 aerogels heat-treated at different temperatures.

sample	Specific surface area (m^2/g)	Average pore diameter (nm)	Pore volume (cm^3/g)	Average micropore diameter by HK method (nm)
ASCE-25	980.8	12.70	3.97	0.902
CSCE-25	732.2	14.97	1.94	0.652
RSCE-25	961.9	13.80	3.53	0.871
ASCE-700	856.7	21.20	3.64	0.604
CSCE-700	641.0	17.21	2.24	0.591
RSCE-700	915.9	17.07	3.24	0.918
ASCE-1000	350.8	20.92	1.67	0.627
CSCE-1000	174.3	19.38	0.82	0.626
RSCE-1000	258.6	19.71	1.08	0.626

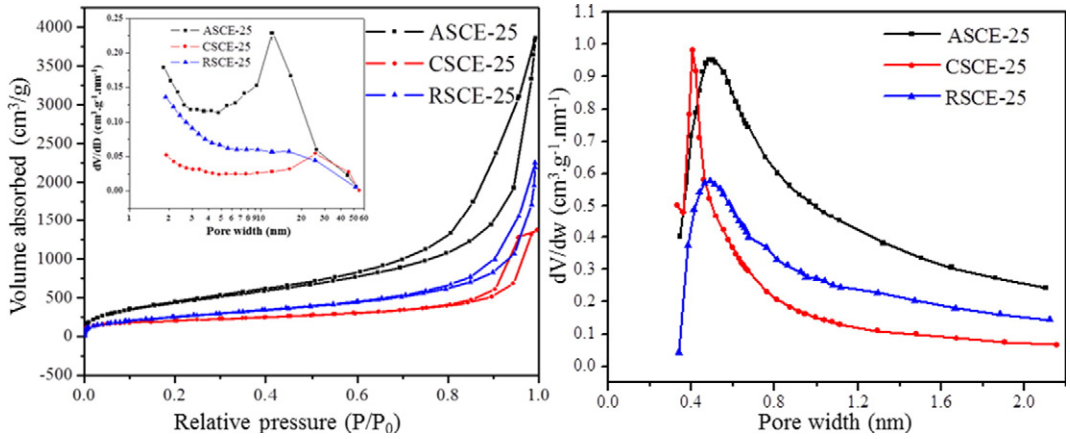

Fig. 9. Nitrogen sorption isotherms (left) and micropore analysis using Horvath-Kawazoe method (right) of as-dried SiO_2 aerogels derived from different drying methods. Insets: the corresponding BJH desorption pore size distributions.

size and an increase in temperature. That is to say, the small silica primary particles dissolve in the solution and begin to precipitate on the surface of the large gel skeleton, as is shown in Fig. 4. Thus, in the RSCE method, when the precursor solution is placed under high-temperature and high-pressure conditions in the vessel, the small silica particles dissolve and precipitate on the large secondary particles with multiple pores including Types I, II, and III. (Note that Type I refers to the pores between the primary particles, Type II refers to the pores that are larger than the secondary particles, and Type III refers to the pores that are smaller than the secondary particles) [28]. According to the pore size distributions of the three as-dried samples in Fig. 9, it is found that the most probable pore diameter for the ASCE-25 is ca. 15 nm, and it is much more intense than the RSCE-25 sample. This phenomenon further verifies that the existence of three types of pores within the RSCE-sample. Thus, when it is heated, the energy can be partly consumed for structural adjustment for the RSCE-25 sample due to the hierarchical pores. SEM images in Fig. 7(c) and (f) also provide similar evidences. There are also some large pores for the RSCE-25 sample except for the main mesopores, however, after heat treatment at 700 °C, the structures become more homogeneous with the disappearance of the large pores. Therefore, the RSCE sample undergoes the dissolution-precipitation process, possessing a substantially smaller bulk density and a higher porosity, which also results in the inhibition of SiO_2 crystallization within the sample.

Fig. 5 shows the FT-IR spectra of the silica aerogels derived from different supercritical drying methods and heat-treatment temperatures. For the as-dried ASCE and RSCE samples, the peaks at 1080 and 466 cm^{-1} represent the symmetrical stretching and bending vibrations of the Si—O—Si groups, respectively [29]. The peak at 794 cm^{-1} is related to the antisymmetric stretching vibration of the Si—O—Si groups, and the intense peak at 3421 cm^{-1} is the characteristic peak for O—H [6]. Adsorbed water molecules show a peak at approximately 1633 cm^{-1}, and the weak peak appearing around 1396 cm^{-1} is attributed to the —CH stretching modes of the non-hydrolyzed ethoxy groups [30]. The bands at 2981, 2934 and 2901 cm^{-1} are attributed to the —CH symmetric stretching vibration and asymmetric stretching vibration, and the band at approximately 1446 cm^{-1} is due to the other —CH stretching [30–32]. The peak at 565 cm^{-1} is due to the stretching vibration of Si—O—Si with defects, and the 971 cm^{-1} peak is related to the —Si—OH stretching vibration. As shown in Fig. 5(b), there are only peaks corresponding to Si—O—Si and —Si—OH, many other peaks are absent, such as those of the —CH vibrations, which indicates that these groups decomposed during heat treatment at 700 °C, as follows:

$$\equiv Si-O-C_2H_5 + 3O_{2(g)} \rightarrow \equiv Si-OH + 2CO_{2(g)} + 2H_2O_{(g)} \quad (4)$$

Furthermore, after the heat treatment at 1000 °C, the –OH is also consumed to form the -Si-O-Si bond, as shown by the following reaction:

$$\equiv Si-OH + HO\text{-}Si \equiv \rightarrow \equiv Si-O-Si \equiv + H_2O_{(g)} \quad (5)$$

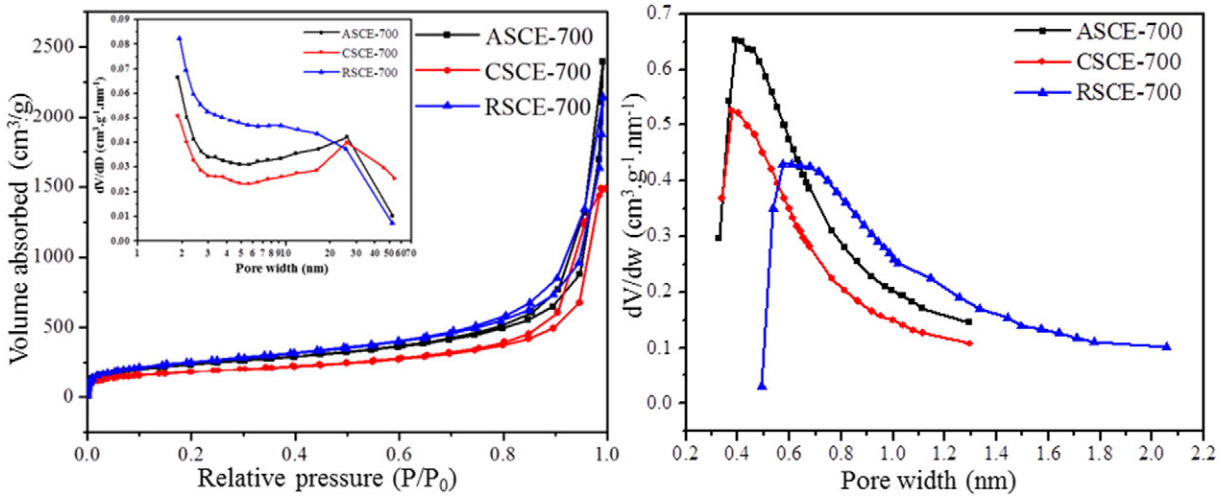

Fig. 10. Nitrogen sorption isotherms (left) and micropore analysis using Horvath-Kawazoe method (right) of SiO_2 aerogels derived from different drying methods which are heat treated at 700 °C.

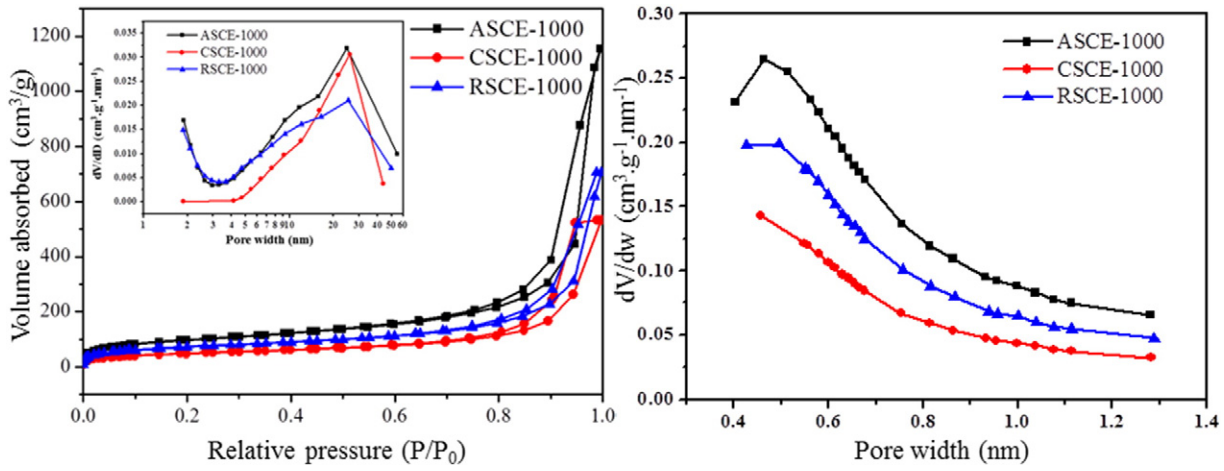

Fig. 11. Nitrogen sorption isotherms (left) and micropore analysis using Horvath-Kawazoe method (right) of SiO_2 aerogels derived from different drying methods which are heat treated at 1000 °C.

For the CSCE sample, the apparent difference is that the peaks corresponding to the —CH vibration are much weaker than those observed with the ASCE and RSCE methods, which may be due to the longer supercritical drying time that provides a longer time for the $—OC_2H_5$ reactions of the wet gel in the vessel.

Fig. 6 presents the TG and DSC curves of the as-dried SiO_2 composite aerogel derived from different supercritical drying methods. The thermogram profiles of the three samples can be divided into three main regions: (1) 20–200 °C; (2) 200–600 °C and (3) 600–1200 °C. It is observed that the RSCE and ASCE samples exhibit similar thermogram files, whereas they are substantially different from the CSCE thermogram. The first region is caused by the evolution of physically adsorbed ethanol and water within the pores, combined with a broad endothermic peak at ca. 100 °C [32,33]. Because the ASCE and RSCE samples experience a significantly higher temperature during the supercritical drying process, the hydrophobic property is, therefore, obtained because of the consumption of the hydrophilic groups, including the —OH. Thus, the mass loss in the first region is much smaller than that of the CSCE sample. The second region is caused by the decomposition of organic groups, such as $—CH_3$ and $—C_2H_5$, which generates gases including H_2O and CO_2. This region contains the majority of the total weight loss, along with a weak exothermic peak at ca. 460 °C; this peak is not observed for the CSCE sample. This result is consistent with the former FTIR analysis, which indicates that the quantity of the organic groups is substantially less than the quantity in the other two samples. It is worth noting that in the third region, there is some weight gain, rather than weight loss, and two weak, broad exothermic peaks are observed at ca. 900 °C. These peaks are caused by the —OH decomposition, as shown in reaction 5. The weight gain in this region stems from nitrogen adsorption within the pores, while the skeleton shrinks and solidifies at elevated temperatures.

Fig. 7 shows the microstructures of the silica aerogels derived from different drying methods and heat-treatment temperatures. The images are shown at 20000–45000× magnification with a 200-nm scale bar present on the left of each image. It is found that all of the as-prepared aerogels present a framework that is similar to strings of pearls, and the particles are distinguishable [34]. The ASCE-25 and CSCE-25 are similar, and show an open nanostructure with visible pores smaller than 100 nm; the diameters of the silica particles are primarily in the range of 20 to 30 nm. Some pores with diameters larger than 200 nm exist in the CSCE-25 sample. The RSCE-25 has a substantially more open structure and a great number of pores larger than 200 nm than the two conventional samples. This is caused by the inhomogeneous growth of the silica sols within the vessel at a high temperature and a high pressure, which also resulting in the aforementioned three types of pores within the structure. The gel skeletons are strengthened under the more moderate conditions of the conventional aging and solvent exchange procedures for the ASCE and CSCE samples. With heating to a temperature < 700 °C, the porous silica lattices are clearly visible, but portions of the aerogels contain a greater density of rounded clusters of silica [26]. The diameters of the silica particles change little, indicating good thermal stability of silica aerogels at high temperatures. It is found that some of the pores with diameters larger than 200 nm increase in the CSCE-700 sample, which can be explained by the volume shrinkage and pore collapse [21]. With further heat treatment at 1000 °C, the ASCE-1000 exhibits a disordered, porous structure typical of a colloidal gel, and the nanoparticles are uniformly distributed to form a framework surrounded by irregular pores. The CSCE-1000 possesses some dense regions at such an elevated temperature, and the nanoparticles appear to grow close to each other, forming substantially fewer pores. On the other hand, the RSCE-1000 sample remains composed of homogeneous nanoparticles and nanopores, which are favorable for applications in thermal insulations and chemical sensors at elevated temperatures.

Fig. 8 shows the TEM images and diffraction rings of the silica aerogels from different drying methods, which are heat treated at 1000 °C. Note that Fig. 8(b), (e) and (h) are higher magnifications of Fig. 8(a), (d) and (g). In combination with the aforementioned discussions, the TEM images reveal that the networks of the resulting aerogels consist of homogeneous and connected spheroidal particles with many surrounding nanopores. According to the schematic diagram in Fig. 4, the specific surface area of the silica aerogels can be calculated as follows:

$$S = N \times 4\pi R_0^2 = \frac{4\pi R_0^2}{\frac{4}{3}\pi R_0^3 \times \rho} = \frac{6}{\rho(2R_0)} \tag{6}$$

Table 2
Thermal performances parameters of different fiber reinforced RSCE SiO_2 aerogel composites.

Reinforcement	Weight increase [a]/%	Density/(g cm^{-3})	Thermal conductivity/(W m^{-1} K^{-1})	Thermal diffusivity/(mm^2 s^{-1})	Specific heat capacity/(MJ m^{-3} K^{-1})
Silica-rich fiber	38–45	0.20	0.028	0.631	0.044
Glass fiber	52–55	0.20	0.027	0.812	0.033
Basalt fiber	25–30	0.27	0.027	0.497	0.054

a: weight gain of the fiber reinforced aerogel composite based on the fiber mass.

where N is the number of primary particles per unit of the aerogel, ρ is the skeleton density (2.05 g/cm^3) of the silica particles and R_0 is the radius of the primary particles. Thus the diameters of the secondary particles can be obtained using the following equation [35]:

$$2R_0 = \frac{6}{\rho S} \quad (7)$$

According to Table 1, the specific surface areas of the ASCE-1000, CSCE-1000 and RSCE-1000 are 350.76 m^2/g, 174.32 m^2/g and 258.57 m^2/g, respectively; thus, the diameters of the secondary particles are 8.1 nm, 16.4 nm and 11.0 nm, respectively. These results are in agreement with the TEM results that show that the CSCE-1000 sample has the largest secondary particles, as indicated by Fig. 8(e). It seems that the particle size of the CSCE aerogels after 1000 °C treatment increases obviously due to the grain growth, which is not consistent with the XRD result in Fig. 3d. This is because since the specific surface area of the CSCE-25 sample is the lowest among the three as-dried samples (Table 1), the primary particle diameter is larger than that of the other two (Eq. (7)). Thus, the actual grain growth of the as-dried CSCE sample is not as obvious as the TEM shows. In addition, although the grain growth is observed, the SAED pattern (Fig. 8(f)) exhibits some diffraction rings, which is a convincing evidence for its amorphous state. Therefore, the CSCE-1000 sample still highly porous with mesoporosity and a non-crystalline structure after heat treatment at a maximum temperature of 1000 °C, which is actually consistent with the results of the XRD patterns [36]. On the other hand, the accuracy of the XRD measurement is limited for samples with part crystallization, thus maybe the diffraction peaks couldn't be detected for the CSCE-1100 sample due to the low crystallization of the sample. With further heat treatment at 1200 °C, the cristobalite phase is obvious in the CSCE sample (Fig. S4).

Figs. 9–11 exhibits the nitrogen sorption isotherms and the pore size distribution of the silica aerogels from different drying methods, which are heat-treated at different temperatures. Both the ASCE and RSCE samples exhibit a hybrid of type II and type IV isotherms, which is caused by the range of pores extending from the mesoporous region to the macroporous region, as is justified by the SEM images. All the curves corresponding to the CSCE samples belong to type IV with a type H1 hysteresis loop, according to the IUPAC classification, which is characteristic of a mesoporous structure with cylindrical pores [37–40]. This phenomenon indicates that some large pores occur in the ASCE and RSCE samples, while the pores in the CSCE samples are relatively homogenous. The presence of some pores larger than 200 nm in CSCE-700, as indicated by Fig. 7(e), suggests an apparent weakening of the saturation region. The desorption cycles for all of the isotherms have a hysteresis loop, which is generally attributed to the capillary condensation that occurs in mesopores. The pore diameters of the peaks for the RSCE-25 and RSCE-700 samples are not apparent, as shown in the top left insets; after heat treated at 1000 °C, the peak shifts to ca. 25 nm. The pore diameter of the peak for the ASCE samples shifts from ca. 15 nm to approximately 25 nm, which is consistent with the results in Table 1. For heat treatments at 700 °C and 1000 °C, the peaks remain nearly the same for the CSCE samples. The most probable micropore diameters for the ASCE and CSCE samples are 0.5 nm and 0.4 nm, respectively, whereas the pore diameter ranges from 0.5 nm to 0.6 nm for the RSCE sample, justifying the results of the average micropore diameter by the HK method, as indicated by Table 1. According to the data in Table 1, it is evident that the specific surface areas decrease with an increase in the heat treatment temperature, which is due to the structural adjustment, damage to the porous network and shrinkage of the pore structure, as is shown in the SEM images [41]. The BET specific surface areas of the CSCE samples possess the smallest values, regardless of the heat treatment temperatures. This finding is supported from the fact that the secondary particles of the CSCE samples first appear at elevated temperatures, as indicated by the TEM results. It is noted here that ASCE-25 has a larger BET specific surface area (980.8 m^2/g) than the other two samples, justifying the homogenous structures in the SEM images. The BET specific surface area of RSCE-25 is also as high as 961.9 m^2/g, which is much higher than the values of different types of aerogels [24–26,42]. After heat treatment at 700 °C, the RSCE sample has a large specific surface area (915.9 m^2/g), which is even larger than the value for ASCE-700, and it is favorable to thermal insulations and catalyst barriers at elevated temperatures. After further heat treatment at 1000 °C, the specific surface area of the RSCE-1000 sample is still as large as 258.57 m^2/g, indicating a good thermal stability at elevated temperatures. The pore volumes of the ASCE-25, CSCE-25 and RSCE-25 are 3.97 cm^3/g, 1.94 cm^3/g and 3.53 cm^3/g, respectively, and are comparable to the values from reference [24]. For the ASCE-25, CSCE-25 and RSCE-25, respectively, the bulk densities are 0.14 g/cm^3, 0.20 g/cm^3 and 0.09 g/cm^3, and the porosities are 93.2%, 91.2% and 95.6%, respectively; thus, it can be calculated that the corresponding pore volumes are 6.66 cm^3/g, 4.56 cm^3/g and 10.62 cm^3/g; these results are significantly higher than the testing results. Therefore, the total pore volume measured from the N_2 adsorption analysis is largely underestimated, and a large fraction of macropores is ignored because of the limitations of this method. As is shown in Table 2, the thermal conductivities of the different fiber reinforced RSCE SiO_2 aerogel composites are as low as 0.028 W m^{-1} K^{-1}, 0.027 W m^{-1} K^{-1} and 0.027 W m^{-1} K^{-1}, respectively, comparable to the ASCE (0.027 W m^{-1} K^{-1}, 0.029 W m^{-1} K^{-1}, 0.031 W m^{-1} K^{-1}) and CSCE aerogel composites (0.027 W m^{-1} K^{-1}, 0.028 W m^{-1} K^{-1}, 0.034 W m^{-1} K^{-1}), which appear suitable for efficient insulation uses.

4. Conclusions

Monolithic silica aerogels are prepared using the TEOS as precursor via an RSCE method. This new RSCE method offers many distinct advantages including shortening the fabrication time to as low as 6 h, producing no toxic waste, largely saving preparation cost. The textural and physical characteristics of RSCE-samples are compared with the conventional ASCE and CSCE samples. All the as-dried SiO_2 samples derived from different methods are essentially amorphous, and SiO_2 crystallization first occurs for the ASCE sample at 1100 °C. The nanoparticles appear to grow and close to each other containing much less pores within the CSCE samples, thus resulting in the smallest specific surface area at elevated temperatures. The average pore diameters of the as-dried ASCE, CSCE and RSCE samples are 12.70 nm, 14.97 nm and 13.80 nm, respectively, which is consistent with the TEM results. The specific surface area of the as-dried RSCE silica aerogel is as large as 915.9 m^2/g after 700 °C, which is even larger than that of the other two samples. The thermal conductivities of the different fiber reinforced RSCE SiO_2 aerogel composites are as low as ca. 0.027 W m^{-1} K^{-1}, comparable to the ASCE and CSCE aerogel composites. The RSCE method can also be well applied to the fabrication of aerogels based on other precursor recipes, and it can be applied to many applications such as thermal insulations, chemical sensors and catalyst barriers.

Acknowledgments

This work was financially supported by the Industry Program of Science and Technology Support Project of Jiangsu Province (BE2014128), the clinical medical special Program of Science and Technology Project of Jiangsu Province (BL2014074), the Prospective Joint Research Program of Jiangsu Province (BY2015005-01), the Major Program of Natural Science Fund in Colleges and Universities of Jiangsu Province (15KJA430005), China Postdoctoral Science Foundation (2015M570442), the Aeronautical Science Foundation of China (201452T4001), the Program for Innovative Research Team in University of Ministry of Education of China (No.IRT_15R35), China Postdoctoral Science Foundation (2015M570442), Natural Science Foundation of Jiangsu Province (BK20161003), Jiangsu Collaborative Innovation Center for Advanced Inorganic Function Composites and the Priority Academic Program Development of Jiangsu Higher Education

Institutions, A Project Funded by the Brand Major Program Development of Jiangsu Higher Education Institutions (PPZY2015B128). Any opinions, findings, and conclusions or recommendations expressed in this paper are those of the authors and do not necessarily reflect the views of these programs.

Appendix A. Supplementary data

Supplementary data to this article can be found online at http://dx.doi.org/10.1016/j.powtec.2017.01.067.

References

[1] W.W. Bao, F.Y. Guo, H.F. Zou, S.C. Gan, X.C. Xu, K.Y. Zheng, Powder Technol. 249 (2013) 220–224.
[2] G.M. Gao, D.R. Liu, H.F. Zou, L.C. Zou, S.C. Gan, Powder Technol. 197 (2010) 283–287.
[3] Y. Fazli, E. Kulani, K. Khezri, H. Alijani, PMMA-grafted silica aerogel nanoparticles via in situ SR&NI ATRP: grafting through approach, Microporous Mesoporous Mater. 214 (2015) 70–79.
[4] Z.X. Lu, Z.S. Yuan, Q. Liu, Z.J. Hu, F. Xie, M. Zhu, Multi-scale simulation of the tensile properties of fiber-reinforced silica aerogel composites, Mater. Sci. Eng. A 625 (2015) 278–287.
[5] Q. Lei, H.H. Song, X.H. Chen, M.C. Li, A. Li, B. Tang, D. Zhou, Effects of graphene oxide addition on the synthesis and supercapacitor performance of carbon aerogel particles, RSC Adv. 6 (2016) 40683–40690.
[6] L. Zhong, X.H. Chen, H.H. Song, K. Guo, Z.J. Hu, Highly flexible silica aerogels derived from methyltriethoxysilane and polydimethylsiloxane, New J. Chem. 39 (2015) 7832–7838.
[7] U. Zulfiqar, T. Subhani, S.W. Husain, Synthesis and characterization of silica nanoparticles from clay, J. Asian Ceram. Soc. 4 (2015) 91–96.
[8] L. Zhong, X.H. Chen, H.H. Song, K. Guo, Z.J. Hu, Synthesis of monolithic zirconia aerogel via a nitric acid assisted epoxide addition method, RSC Adv. 4 (2014) 31666–31671.
[9] A. Mohammadi, J. Moghaddas, Synthesis, adsorption and regeneration of nanoporous silica aerogel and silica aerogel-activated carbon composites, Chem. Eng. Res. Des. 94 (2015) 475–484.
[10] A. Du, B. Zhou, Z.H. Zhang, J. Shen, A special material or a new state of matter: a review and reconsideration of the aerogel, Materials 6 (2013) 941–968.
[11] C.A. Ferreiro-Rangel, L.D. Gelb, Investigation of the bulk modulus of silica aerogel using molecular dynamics simulations of a coarse-grained model, J. Phys. Chem. B 117 (2013) 7095–7105.
[12] Z. Li, X. Cheng, S. He, X. Shi, H. Yang, Characteristics of ambient-pressure-dried aerogels synthesized via different surface modification methods, J. Sol-Gel Sci. Technol. 76 (2015) 138–149.
[13] Z. Shao, X. He, Z. Niu, T. Huang, X. Cheng, Y. Zhang, Ambient pressure dried shape-controllable sodium silicate based composite silica aerogel monoliths, Mater. Chem. Phys. 162 (2015) 346–353.
[14] G. Wu, J. Yang, D. Wang, R. Xu, K. Amine, C. Lu, A novel route for preparing mesoporous carbon aerogels using inorganic templates under ambient drying, Mater. Lett. 115 (2014) 1–4.
[15] Z. Li, X. Cheng, S. He, D. Huang, H. Bi, H. Yang, Preparation of ambient pressure dried MTMS/TEOS co-precursor silica aerogel by adjusting NH_4OH concentration, Mater. Lett. 129 (2014) 12–15.
[16] G.M. Pajonk, M. Repellin-Lacroix, S. Abouarnadasse, J. Chaouki, D. Klavana, From sol-gel to aerogels and cryogels, J. Non-Cryst. Solids 121 (1990) 66–67.
[17] X.D. Wu, G.F. Shao, S. Cui, L. Wang, X.D. Shen, Synthesis of a novel Al_2O_3—SiO_2 composite aerogel with high specific surface area at elevated temperatures using inexpensive inorganic salt of aluminum, Ceram. Int. 42 (2015) 874–882.
[18] L. Xu, Y.G. Jiang, J.Z. Feng, J. Feng, C.W. Yue, Infrared-opacified Al_2O_3—SiO_2 aerogel composites reinforced by SiC-coated mullite fibers for thermal insulations, Ceram. Int. 41 (2015) 437–442.
[19] G.Q. Zu, J. Shen, L.P. Zou, W.Q. Wang, Y. Lian, Z.H. Zhang, A. Du, Nanoengineering super heat-resistant, strong alumina aerogels, Chem. Mater. 25 (2013) 4757–4764.
[20] A.M. Anderson, C.W. Wattley, M.K. Carroll, Silica aerogels prepared via rapid supercritical extraction: effect of process variables on aerogel properties, J. Non-Cryst. Solids 355 (2009) 101–108.
[21] Y. Shen, A. Du, X.L. Wu, X.G. Li, J. Shen, B. Zhou, Low-cost carbon nanotube aerogels with varying and controllable density, J. Sol-Gel Sci. Technol. 79 (2016) 76–82.
[22] Y. Kong, X.D. Shen, S. Cui, M.H. Fan, Use of monolithic silicon carbide aerogel as a reusable support for development of regenerable CO_2 adsorbent, RSC Adv. 4 (2014) 64193–64199.
[23] X.D. Wu, Y. Zhong, Y. Kong, G.F. Shao, S. Cui, L. Wang, J. Jiao, X.D. Shen, Preparation and characterization of C/Al_2O_3 composite aerogel with high compressive strength and low thermal conductivity, J. Porous. Mater. 22 (2015) 1235–1243.
[24] L.B. Brown, A.M. Anderson, M.K. Carroll, Fabrication of titania and titania-silica aerogels using rapid supercritical extraction, J. Sol-Gel Sci. Technol. 62 (2012) 404–413.
[25] N. Dunn, M.K. Carroll, A.M. Anderson, Characterization of alumina and nickel-alumina aerogels prepared via rapid supercritical extraction, Polym. Prepr. 52 (2011) 250–251.
[26] A.M. Anderson, M.K. Carroll, E.C. Green, J.T. Melville, M.S. Bono, Hydrophobic silica aerogels prepared via rapid supercritical extraction, J. Sol-Gel Sci. Technol. 53 (2010) 199–207.
[27] A.K. Shchekin, A.I. Rusanov, Generalization of the Gibbs-Kelvin-Köhler and Ostwald-Freundlich equations for a liquid film on a soluble nanoparticle, J. Chem. Phys. 129 (2008) 154116.
[28] L. Esquivias, J.R. Ortega, C.B. Solano, N.D. Rosa-Fox, Structural models of dense aerogels, J. Non-Cryst. Solids 225 (1998) 239–243.
[29] S. He, Y. Bi, Y. Zhang, H. Cao, X. Shi, X. Luo, L. Zhang, One-pot synthesis and characterization of acid-catalyzed melamine formaldehyde/SiO_2 aerogel via sol–gel technology, J. Sol-Gel Sci. Technol. 74 (2015) 175–180.
[30] Y. Özbakır, Z. Ulker, C. Erkey, Monolithic composites of silica aerogel with poly(methyl vinyl ether) and the effect of polymer on supercritical drying, J. Supercrit. Fluids 105 (2015) 108–118.
[31] X. Han, F. Williamson, G.A. Bhaduri, A. Harvey, L. Šiller, Synthesis and characterization of ambient pressure dried composites of silica aerogel matrix and embedded nickel nanoparticles, J. Supercrit. Fluids 106 (2015) 140–144.
[32] L. Durães, A. Maia, A. Portugal, Effect of additives on the properties of silica based aerogels synthesized from methyltrimethoxysilane (MTMS), J. Supercrit. Fluids 106 (2015) 85–92.
[33] L.S. White, M.F. Bertino, G. Kitchen, J. Young, C. Newton, R. Al-Soubaihi, S. Saeed, K. Saoud, Shortened aerogel fabrication times using an ethanol-water azeotrope as a gelation and drying solvent, J. Mater. Chem. A 3 (2015) 762–772.
[34] Y. Kong, Y. Zhong, X.D. Shen, S. Cui, J. Zhang, M. Yang, Synthesis and characterization of monolithic carbon/silicon carbide composite aerogels, J. Porous. Mater. 20 (2013) 845–849.
[35] J.Z. Feng, J. Feng, C.R. Zhang, Shrinkage and pore structure in preparation of carbon aerogels, J. Sol-Gel Sci. Technol. 59 (2011) 371–380.
[36] R. Xiong, X.L. Li, H.M. Ji, X.H. Sun, J. He, Thermal stability of ZrO_2—SiO_2 aerogel modified by Fe(III) ion, J. Sol-Gel Sci. Technol. 72 (2014) 496–501.
[37] A. Du, B. Zhou, J. Shen, J.Y. Cui, Y.H. Zhong, C.Z. Liu, Z.H. Zhang, G.M. Wu, A versatile sol–gel route to monolithic oxidic gels via polyacrylic acid template, New J. Chem. 35 (2011) 1096–1102.
[38] X.L. Li, Y. Jiao, H.M. Ji, X.H. Sun, The effect of propylene oxide on microstructure of zirconia monolithic aerogel, Integr. Ferroelectr. 146 (2013) 122–126.
[39] J. He, X.L. Li, D. Su, H.M. Ji, X.J. Wang, Ultra-low thermal conductivity and high strength of aerogels/fibrous ceramic composites, J. Eur. Ceram. Soc. 36 (2016) 1487–1493.
[40] A. Du, B. Zhou, J. Shen, S.F. Xiao, Z.H. Zhang, C.Z. Liu, M.X. Zhang, Monolithic copper oxide aerogel via dispersed inorganic sol-gel method, J. Non-Cryst. Solids 335 (2009) 175–181.
[41] F. Hurwitz, H. Guo, R. Rogers, E. Sheets, D. Miller, K. Newlin, M. Shave, A. Palczer, M. Cox, Influence of Ti addition on boehmite-derived aluminum silicate aerogels: structure and properties, J. Sol-Gel Sci. Technol. 64 (2012) 367–374.
[42] S.K. Estok, T.A. Hughes, M.K. Carroll, A.M. Anderson, Fabrication and characterization of TEOS-based silica aerogels prepared using rapid supercritical extraction, J. Sol-Gel Sci. Technol. 70 (2014) 371–377.